

Intention-aware Denoising Diffusion Model for Trajectory Prediction

Chen Liu, Shibo He, Haoyu Liu, Jiming Chen

Abstract—Trajectory prediction is an essential component in autonomous driving, particularly for collision avoidance systems. Considering the inherent uncertainty of the task, numerous studies have utilized generative models to produce multiple plausible future trajectories for each agent. However, most of them suffer from restricted representation ability or unstable training issues. To overcome these limitations, we propose utilizing the diffusion model to generate the distribution of future trajectories. Two cruxes are to be settled to realize such an idea. First, the diversity of intention is intertwined with the uncertain surroundings, making the true distribution hard to parameterize. Second, the diffusion process is time-consuming during the inference phase, rendering it unrealistic to implement in a real-time driving system. We propose an **Intention-aware Denoising Diffusion Model (IDM)**, which tackles the above two problems. We decouple the original uncertainty into **intention uncertainty** and **action uncertainty**, and model them with two dependent diffusion processes. To decrease the inference time, we reduce the variable dimensions in the intention-aware diffusion process and restrict the initial distribution of the action-aware diffusion process, which leads to fewer diffusion steps. To validate our approach, we conduct experiments on **Stanford Drone Dataset (SDD)** and **ETH/UCY dataset**. Our methods achieve state-of-the-art results, with an **FDE of 13.83 pixels on SDD dataset and 0.36 meters on ETH/UCY datasets**. Compared with the original diffusion model, **IDM reduces inference time by two-thirds**. Interestingly, our experiments further reveal that **introducing intention information is beneficial in modeling the diffusion process of fewer steps**.

Index Terms—trajectory prediction, diffusion models

I. INTRODUCTION

ALTHOUGH high-level autonomous driving systems can significantly enhance our convenience, it remains a challenging task to maintain its security [1]. As mentioned in [2]–[4], self-driving vehicles must anticipate the future movements of surrounding agents (including vehicles and pedestrians) in order to plan proactive motions and avoid collision with them. Therefore, trajectory prediction plays a crucial role in autonomous driving systems [5].

Traditional deterministic trajectory prediction methods aim to provide a single future trajectory for each agent [6]–[9]. However, it has been recognized that not all relevant clues, such as the intentions and habits of the agents, can be fully acquired. Consequently, there may exist multiple plausible future trajectories for an agent [10], which can be

Chen Liu, Shibo He, Jiming Chen are with State Key Lab. of Industrial Control Technology, Zhejiang University, Hangzhou 310027, China. Email: {liu777ch, s18he, cjm}@zju.edu.cn. Haoyu Liu is with Fuxi AI Lab, NetEase Games, Hangzhou 310052, and also with State Key Laboratory of Industrial Control Technology, Zhejiang University, Hangzhou 310027, China. Email: liuhaoyu03@corp.netease.com.

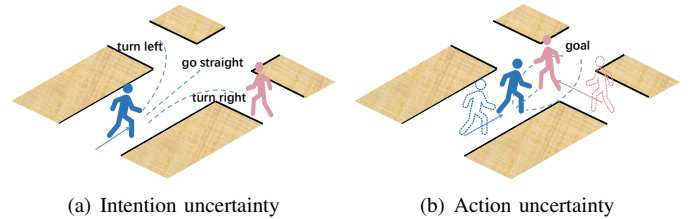


Fig. 1. Two kinds of uncertainty: (a) A pedestrian may turn left, turn right, or proceed straight based on his own will; (b) A pedestrian with a deterministic goal can also choose different paths in order to avoid collisions with their surroundings.

ignored by these deterministic methods. To address this issue, probabilistic trajectory prediction attempts to generate multiple predictions to encompass all possible outcomes, and it has garnered growing interest in recent years [11].

Previous studies have investigated different generative models for probabilistic trajectory prediction, including noise-based models, bivariate-Gaussian (BG)-based models, conditional variational autoencoder (CVAE)-based models, and generative adversarial network (GAN)-based models [12]. Noise-based models, used by Gupta et al., Thiede et al., and Deo et al. [13]–[15] involve injecting random noise into neural networks to generate multiple future trajectories and training the networks using a variety loss. However, the variety loss fails to penalize unrealistic trajectories, resulting in the inability to accurately describe the true distribution of possible trajectories [16]. BG-based models, used by Alal et al. [17] and Mohamd et al. [18] assume that future positions follow a bivariate-Gaussian distribution and estimate the distribution parameters using maximum likelihood estimation. However, real-world trajectories may follow more complex distributions, leading to the capped performance of their methods [12]. CVAE-based models aim to incorporate uncertainty into the predictions by introducing a latent distribution [19]–[22]. Nevertheless, CVAE is observed to generate unnatural trajectories due to its limited ability to model complex distributions [23]. Additionally, GANs are employed to fit parameterized probability distributions [24]–[26]. However, the unstable training procedure of GANs hinders their practical development [27]. In summary, all these generative models suffer from limited ability to represent sophisticated trajectory distributions or unstable training processes.

Recently, diffusion models have shown their potential in overcoming two aforementioned limitations and have gained prominence among generative models [28]–[30]. Compared with CVAE and BG-based models, diffusion models offer

greater representation ability, as they can generate complex distributions through a series of steps [31]. Additionally, the training process of diffusion models is more stable compared to GANs [32]. As a result, diffusion models have achieved state-of-the-art performance in various domains, including image synthesis [28]–[30], video generation [33], [34] and audio processing [35], [36]. Considering the aforementioned advantages of diffusion models, we propose adopting diffusion models for the trajectory prediction problem. However, two main challenges need to be addressed to realize this idea.

How to clearly model the uncertainty of multimodal future? The uncertainty of agent movement is significantly influenced by both internal stimulus and external environmental factors. For example, at a crossroad, individuals may choose to turn left, turn right, or proceed straight based on their intentions, as depicted in Fig. 1(a). Furthermore, even when the goal (endpoint) is deterministic, they may select different paths. Fig. 1(b) illustrates a scenario where an individual intends to go straight but adjusts their movement to the left or right to avoid a collision with another person. It has been recognized in [10] that the future trajectory distribution should be multimodal, with each mode representing a different intention of the agent. Applying the original diffusion model to this task would neglect the multimodal property of the trajectory [32], as it only models the uncertainty of paths without considering intention information. As a result, it may produce stochastic and unnatural predictions.

How to enhance the efficiency of diffusion model? The diffusion model typically performs poorly in terms of time efficiency, resulting in a significant drawback when applied to trajectory prediction for autonomous driving systems. The considerable time consumption can be attributed to two factors. Firstly, the diffusion model follows a Markov chain, where the ground truth distribution is transformed into a prior Gaussian noise distribution by injecting noises step by step. To ensure that the prior noise distribution follows a Gaussian distribution, the diffusion process entails a large number of steps [37]. Consequently, during the reverse process, obtaining the ground truth distribution from the Gaussian noise also necessitates a large number of denoising steps, resulting in low efficiency. Secondly, the inefficiency is further exacerbated by the high dimensions of data involved in the diffusion process [38]. Dealing with high-dimensional data requires more computational resources and time, making the overall process slower.

To address the aforementioned challenges, we propose an intention-aware diffusion model called IDM for trajectory prediction. Our approach involves decoupling the uncertainty of trajectory prediction into intention uncertainty and action uncertainty. To model the intention uncertainty, we utilize a diffusion process to estimate the distribution of the agent’s goal. For action uncertainty, we employ another diffusion process to estimate the distribution of paths conditioned on a specific goal. During the prediction stage, we first infer multiple possible goals of the agent and then generate trajectories conditioned on all of these inferred goals. This approach allows for capturing the multimodal nature of the trajectory distribution, which can integrate both intention and action

uncertainties. To enhance computational efficiency, in the goal diffusion process, we consider each trajectory’s endpoint as the particle instead of the entire trajectory, thus reducing the dimension of the data being modeled. In the path diffusion process, rather than using prior Gaussian noise distribution, we propose to estimate the prior noise distribution by a neural network, thereby reducing the number of steps required in the diffusion process. Additionally, we design a corresponding loss function to enable end-to-end training of the two diffusion processes. We evaluate our model on two real-world datasets, and the results demonstrate IDM’s superior performance. It achieves state-of-the-art results in both Average Displacement Error (ADE) and Final Displacement Error (FDE). Compared to traditional denoising diffusion models, our model reduces inference times by two-thirds. Interestingly, we also discover the significance of intention in providing valuable clues for estimating the prior noise distribution accurately. The contributions are summarized as follows:

- We propose a two-stage diffusion model for trajectory generation called IDM, which decouples the uncertainty of trajectory prediction into goal uncertainty and action uncertainty, and model them by two dependent diffusion processes.
- To enhance computational efficiency, we propose a PriorNet for estimating prior noise distribution and utilize a tailored loss function during training, which significantly reduces the required number of steps in the diffusion process. Interestingly, we also find that the goal can provide valuable information for accurate prior distribution noise estimation.
- We perform extensive experiments on two real-world datasets. Our findings show that IDM achieves state-of-the-art detection performance in terms of ADE and FDE. Additionally, IDM significantly reduces inference time by about two-thirds compared to the original diffusion model.

The rest of this paper is organized as follows. In Section II, we provide a comprehensive review of related works on trajectory prediction and diffusion models. Section III formulates the problem and provides preliminary knowledge. Section IV presents a detailed explanation of our proposed method. In Section V, we conduct experiments to assess the performance of our method. Finally, we conclude our study in Section VI.

II. RELATED WORK

A. Trajectory Prediction

Trajectory prediction plays a crucial role in the field of self-driving vehicles. Previous studies in this area can be broadly categorized into three main approaches: physics-based, planning-based, and pattern-based [4].

1) *Physics-based approaches*: Previous works on trajectory prediction use hand-crafted dynamic models based on Newton’s laws of motion. Early approaches often employ methods like autoregressive models [39], Kalman filters [40], and particle filters [41] to make one-step-ahead predictions. These predictions are based on classical kinematic models like the

constant velocity model (CV), the constant acceleration model (CA), the bicycle model and so on [42]–[44]. Other works incorporate map-related contextual clues [45]–[47] and social interaction information [48]–[50] into physics-based models. While these methods perform well under mild conditions, their performance deteriorates over longer prediction horizons due to the absence of future control signals, limiting their applicability to long-term prediction tasks of more than 1 second [1].

2) *Planning-based approaches*: Planning-based approaches assume that agents are rational decision-makers during action. Therefore, they turn the prediction problem into a sequential decision-making problem aimed at finding an optimal motion sequence that minimizes a cost function [4]. The approaches can be classified into forward-planning ones and inverse-planning ones. The forward-planning methods generate plausible trajectories using path planning with hand-crafted cost-function [51]. The interactions among multi-agents are also considered through cooperative planning in joint state-space [52]–[54]. However, these works all predefine an explicit cost or reward function, which sometimes obviates from reality. The inverse planning methods estimate the cost function from all observations via Inverse Reinforcement Learning (IRL) [55]. Other works employ Generative Adversarial Imitation Learning (GAIL) [31] to model the future motion state distribution directly without learning the reward function first [56], [57]. These methods are computationally intensive and consume large training costs.

3) *Pattern-based approaches*: With the development of deep learning, researchers develop approaches that learn trajectory patterns directly from data. Most of the existing deep learning models for trajectory prediction adopt an encoder-decoder architecture [58]. The encoder captures meaningful information for prediction, such as historical trajectories, map information, and states of neighbor agents. To model historical trajectories, previous works utilize sequence modeling techniques like long short-term memory networks (LSTM) [17], [59], temporal convolutional network (TCN) [60], and Transformer [15]. To provide prior knowledge of road structure, the high-definition map can be encoded by rasterization [61] or vectorization [9]. The interactions among multiple agents are often modeled by the social pooling mechanism [62], attention mechanisms [63]–[65] or graph neural networks [18], [66], [67]. The decoder network aggregates all information and generates the eventual predictions. Song et al. focus on the feasibility of predictions, by imposing dynamic and scene-compliant restrictions on the output sequence [68]–[70]. Other works pay attention to stochastic predictions. A common practice is to incorporate a noise signal into the decoder and utilize the variety loss [13] to train the decoder. However, Guo et al. point out that the variety loss can not penalize those unrealistic trajectories, and may generate unfeasible samples during inference [16]. Therefore, the following works turn to adopt generative models. For example, Salzmann et al. firstly propose a Conditional Variational Autoencoder (CVAE) based method Trajectron++ [19], and several works follow the architecture [20]–[22]. Other works apply Generative Adversarial Network (GAN) to trajectory generation [24]–[26].

To generate multimodal trajectories, the latent variable which implies the intention of the agents such as goal endpoints [23], [71] and goal lanes [15], [72] are estimated to enhance the training [10], [73]. However, the CVAE-based methods encounter the performance bottleneck when handling complicated distribution, while the GAN-based methods are trapped in unstable training. In this work, we aim to employ diffusion models to achieve multimodal and stochastic prediction. The most related works to us are [32] and [74]. Our work differs from them in two aspects. Firstly, we consider the multimodal property and devise a goal-aware diffusion process. Secondly, we significantly reduce the number of steps in the diffusion process by estimating the multi-modal prior distribution instead of using the normal distribution assumption, which significantly shortens the inference time.

B. Diffusion Model

Recent years have witnessed the success of diffusion model in various domains such as image synthesis [28]–[30], video generation [33], [34], sequence modeling [75], [76] and audio processing [35], [36]. As a powerful and novel deep generative model, the diffusion model originates from non-equilibrium thermodynamics and is first proposed in [77]. The key concept of the diffusion model is to turn original signals into a known noise distribution by injecting noise gradually and then reverse the process during generation [78]. The denoising process is modeled by a parameterized Markov chain, which can be learned by a neural network. Compared with classical generative models like VAE [79] and GAN [80], the diffusion model shows great potential in representation learning and has a stable training procedure with solid theoretical supports [81]. However, the diffusion model has an inherent weakness of slow generation process [82], which limits its application in real-time scenarios such as autonomous driving. To address this issue, we propose an efficient diffusion model for trajectory prediction, taking inspiration from previous works. Robin et al. propose a diffusion process targeting low-dimension latent features to reduce the cost of training and inference [38]. Therefore, utilizing intention (goal) instead of the whole trajectory to establish the diffusion process can result in significant cost savings. Furthermore, Meng et al. claim that the diffusion process removes signals from high-frequency to low-frequency [37]. In our proposed framework, we assume that the agent’s intention (goal) contains low-frequency information, while the path contains high-frequency information. Therefore, we utilize the predicted goal information to estimate the intermediate distribution with low-frequency signals. This allows us to model the process from the original distribution to this intermediate distribution, effectively reducing the number of steps required in the diffusion process.

III. SYSTEM MODEL

A. Problem Statement

The goal of trajectory prediction is to predict the future locations of agents on the road, such as pedestrians, riders, or vehicles, based on their historical tracepoints. Due to the inherent uncertainty of moving objects, there are many

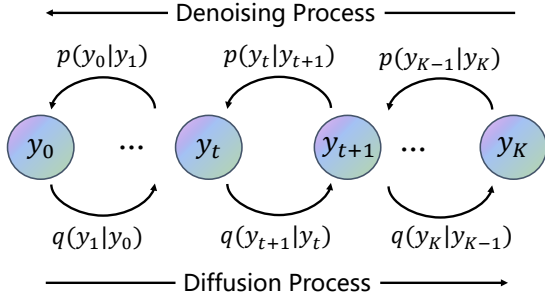


Fig. 2. Denoising Diffusion Probabilistic Model

plausible routes that the agents could follow in the future, so our focus is on generating a trajectory distribution that is as realistic as possible, guided by all available observations. Mathematically, given a target agent with trajectories in the past $x = \{s_t \in \mathbb{R}^2 \mid t = -T_P + 1, -T_P + 2, \dots, 0\}$, where s_t denotes its 2-D locations at time t , and T_P is the time step of trajectory, we aim to predict its future trajectory distribution $y = \{p(s_t) \mid t = 1, 2, \dots, T_Q\}$, where T_Q is the length of prediction, and $p(s_t)$ represents the distribution of all possible locations at time t . In realistic scenario, we could predict \mathcal{K} trajectories $\{y_i \in \mathbb{R}^{T_Q \times 2} \mid i = 1, 2, \dots, \mathcal{K}\}$ in the future. In addition, environmental factors such as historical locations of neighbor agents $e = \{s_t^e \mid t = -T_P + 1, -T_P + 2, \dots, 0\}$, and the map \mathcal{M} can be vectorized [9] to assist the prediction. We summarize all the notations used in our work in Table I.

 TABLE I
 SUMMARY OF NOTATIONS

Symbol	Description
x	The agent's historical trajectory
y	The agent's future trajectory
e	The neighbor's historical trajectory
\mathcal{M}	The map of the scene
T_P	Number of historical steps
T_Q	Number of future steps
\mathcal{K}	Number of future predictions
K	Number of steps in the goal diffusion process
S	Number of steps in the trajectory diffusion process
α_k^g	The diffusion coefficient at k -th step for goal
α_s	The diffusion coefficient at s -th step for trajectory
g_ψ	Encoder with parameters ψ
e_θ	EndNet with parameters θ
μ_ϕ	PriorNet with parameters ϕ
ϵ_φ	PathNet with parameters φ
λ_1	The coefficient for trajectory diffusion loss
λ_2	The coefficient for trajectory prior loss
\mathbf{x}	The context vectors generated by the encoder
\mathbf{c}_k	The goal at k -th step in diffusion process
\mathbf{y}_s	The trajectory at s -th step in diffusion process
\mathbf{c}_0	The ground truth goal
\mathbf{y}_0	The ground truth trajectory

B. Denoising Diffusion Probabilistic Model

Generative models aim to discover the real distribution of observed samples by representing uncertainty through latent variables. Inspired by non-equilibrium thermodynamics, the denoising diffusion probabilistic model (DDPM) describes the distribution of samples as particles in motion, akin to the behavior of particles in thermodynamics. As noise is gradually

added to the observed samples, the distribution of real data, which initially has low uncertainty, transforms into a random distribution with high uncertainty. This transformation process is commonly referred to as the diffusion process or forward process. As shown in Fig 2, the diffusion process is modeled using a parameterized Markov chain:

$$q(\mathbf{y}_{1:K} \mid \mathbf{y}_0) := \prod_{k=1}^K q(\mathbf{y}_k \mid \mathbf{y}_{k-1}) \quad (1)$$

$$q(\mathbf{y}_k \mid \mathbf{y}_{k-1}) := \mathcal{N}(\mathbf{y}_k; \sqrt{1 - \beta_k} \mathbf{y}_{k-1}, \beta_k \mathbf{I})$$

where $\beta_1, \beta_2, \dots, \beta_k$ denote the variance schedulers that control the level of Gaussian noise that is injected into the original signals. On the other hand, the reverse process, also known as the denoising process, involves transforming the noisy distribution back into the sample distribution. This process can also be represented as a Markov chain:

$$p_\theta(\mathbf{y}_{0:K}) := p(\mathbf{y}_K) \prod_{k=1}^K p_\theta(\mathbf{y}_{k-1} \mid \mathbf{y}_k) \quad (2)$$

$$p_\theta(\mathbf{y}_{k-1} \mid \mathbf{y}_k) := \mathcal{N}(\mathbf{y}_{k-1}; \boldsymbol{\mu}_\theta(\mathbf{y}_k, k), \boldsymbol{\Sigma}_\theta(\mathbf{y}_k, k))$$

where the mean $\boldsymbol{\mu}_\theta(\mathbf{x}_k, k)$ and variance $\boldsymbol{\Sigma}_\theta(\mathbf{x}_k, k)$ of reverse transition is learnt by a neural network.

Based on the fixed forward process parameters, We can acquire y_t at any time step as follows:

$$q(\mathbf{y}_k \mid \mathbf{y}_0) = \mathcal{N}(\mathbf{y}_k; \sqrt{\bar{\alpha}_k} \mathbf{y}_0, (1 - \bar{\alpha}_k) \mathbf{I}) \quad (3)$$

using the notations: $\alpha_k := 1 - \beta_k$ and $\bar{\alpha}_k := \prod_{s=1}^k \alpha_s$. It can be seen that the final noised distribution y_k approaches the normal distribution as k increases. A common practice is to set a large step number K , which can result in y_K being equivalent to a normal distribution. By using this setting, we can obtain real samples from the normal distribution through the reverse process.

Our aim is to learn $p_\theta(\mathbf{y}_{k-1} \mid \mathbf{y}_k)$ that match the diffusion process. The training objective is to maximize the likelihood function $\mathbb{E}[\log p_\theta(\mathbf{y}_0)]$, using variational inference:

$$\begin{aligned} \mathbb{E}[\log p_\theta(\mathbf{y}_0)] &= \mathbb{E}_{q(\mathbf{y}_{1:K} \mid \mathbf{y}_0)} \left[\log \frac{p_\theta(\mathbf{y}_{0:K})}{p_\theta(\mathbf{y}_{1:K} \mid \mathbf{y}_0)} \right] \\ &= \mathbb{E}_{q(\mathbf{y}_{1:K} \mid \mathbf{y}_0)} \left[\log \frac{p_\theta(\mathbf{y}_{0:K})}{q(\mathbf{y}_{1:K} \mid \mathbf{y}_0)} \right] \\ &\quad + D_{KL}(q(\mathbf{y}_{1:K} \mid \mathbf{y}_0, \cdot) \parallel p_\theta(\mathbf{y}_{1:K} \mid \mathbf{y}_0)) \end{aligned} \quad (4)$$

then we can maximize the first term called evidence lower bound:

$$ELBO = \mathbb{E}_q \left[\log p(\mathbf{y}_K) + \sum_{k=1}^K \log \frac{p_\theta(\mathbf{y}_{k-1} \mid \mathbf{y}_k)}{q(\mathbf{y}_k \mid \mathbf{y}_{k-1})} \right] \quad (5)$$

since y_K is determined by the real data distribution y_0 and the predefined variance schedulers, it represents a constant

distribution and can be disregarded during training. Therefore, the loss function is defined as follows:

$$\begin{aligned} L(\theta) &= \mathbb{E}_q \left[\sum_{k=1}^K \log \frac{p_\theta(\mathbf{y}_{k-1} | \mathbf{y}_k, \mathbf{y}_0)}{q(\mathbf{y}_k | \mathbf{y}_{k-1})} \right] \\ &= \mathbb{E}_q \left[\sum_{k=1}^K D_{KL}(q(\mathbf{y}_{k-1} | \mathbf{y}_k, \mathbf{y}_0) \| p_\theta(\mathbf{y}_{k-1} | \mathbf{y}_k)) \right] \end{aligned} \quad (6)$$

Indeed, posterior distribution $q(\mathbf{y}_{k-1} | \mathbf{y}_k, \mathbf{y}_0)$ is also a Gaussian distribution:

$$q(\mathbf{y}_{k-1} | \mathbf{y}_k, \mathbf{y}_0) = \mathcal{N}(\mathbf{y}_{k-1}; \tilde{\boldsymbol{\mu}}_k(\mathbf{y}_k, \mathbf{y}_0), \tilde{\boldsymbol{\beta}}_k \mathbf{I}) \quad (7)$$

where the parameters are calculated according to:

$$\begin{aligned} \tilde{\boldsymbol{\mu}}_k(\mathbf{y}_k, \mathbf{y}_0) &= \frac{\sqrt{\bar{\alpha}_{k-1}}\beta_k}{1-\bar{\alpha}_k}\mathbf{y}_0 + \frac{\sqrt{\bar{\alpha}_k}(1-\bar{\alpha}_{k-1})}{1-\bar{\alpha}_k}\mathbf{y}_k \\ &= \frac{1}{\sqrt{\bar{\alpha}_k}} \left(\mathbf{y}_k - \frac{\beta_k}{\sqrt{1-\bar{\alpha}_k}}\epsilon \right) \\ \tilde{\boldsymbol{\beta}}_k &= \frac{1-\bar{\alpha}_{k-1}}{1-\bar{\alpha}_k}\beta_k \mathbf{I}. \end{aligned} \quad (8)$$

where $\epsilon \sim \mathcal{N}(0, \mathbf{I})$. Based on (2), the loss function can be regarded as the KL divergence of two Gaussian distributions. To simplify the optimization, we set $\boldsymbol{\Sigma}_\theta(\mathbf{y}_k, k) = \tilde{\boldsymbol{\beta}}_k$, and reparameterize $\boldsymbol{\mu}_\theta(\mathbf{y}_k, k)$ as:

$$\boldsymbol{\mu}_\theta(\mathbf{y}_k, k) = \frac{1}{\sqrt{\bar{\alpha}_k}} \left(\mathbf{y}_k - \frac{\beta_k}{\sqrt{1-\bar{\alpha}_k}}\epsilon_\theta(\mathbf{y}_k, k) \right) \quad (9)$$

where $y_k = \sqrt{\bar{\alpha}_k}\mathbf{y}_0 + (1-\bar{\alpha}_k)\epsilon$, then the eventual loss is:

$$\begin{aligned} L(\theta) &= \mathbb{E}_q \left[\lambda \|\tilde{\boldsymbol{\mu}}_k(\mathbf{y}_k, \mathbf{y}_0) - \boldsymbol{\mu}_\theta(\mathbf{y}_k, k)\|^2 \right] \\ &\propto \mathbb{E}_q \|\epsilon - \epsilon_\theta(\mathbf{y}_k, k)\|^2 \end{aligned} \quad (10)$$

During inference, we recover original sample y_0 from $y_K \sim \mathcal{N}(0, \mathbf{I})$ step by step according to:

$$y_{k-1} = \frac{1}{\sqrt{\bar{\alpha}_k}} \left(\mathbf{y}_k - \frac{\beta_k}{\sqrt{1-\bar{\alpha}_k}}\epsilon_\theta(\mathbf{y}_k, k) \right) \quad (11)$$

C. Conditional Denoising Diffusion Probabilistic Model

When using the diffusion model for trajectory prediction, it is important to consider the impacts of historical trajectory and environmental information on the future trajectory distribution. Mathematically, we represent all inputs by a context vector \mathbf{x} and aim to analyze the conditional distribution $p_\theta(\mathbf{y}_0 | \mathbf{x})$. The forwarding process is defined as follows:

$$\begin{aligned} q(\mathbf{y}_{1:K} | \mathbf{y}_0, \mathbf{x}) &:= \prod_{k=1}^K q(\mathbf{y}_k | \mathbf{y}_{k-1}) \\ q(\mathbf{y}_k | \mathbf{y}_{k-1}) &:= \mathcal{N}(\mathbf{y}_k; \sqrt{1-\beta_t}\mathbf{y}_{k-1}, \beta_k \mathbf{I}) \end{aligned} \quad (12)$$

while the reverse process is parameterized by:

$$\begin{aligned} p_\theta(\mathbf{y}_{0:K} | \mathbf{x}) &:= p(\mathbf{y}_K | \mathbf{x}) \prod_{k=1}^K p_\theta(\mathbf{y}_{k-1} | \mathbf{y}_k, \mathbf{x}) \\ p_\theta(\mathbf{y}_{k-1} | \mathbf{y}_k, \mathbf{x}) &:= \mathcal{N}(\mathbf{y}_{k-1}; \boldsymbol{\mu}_\theta(\mathbf{y}_k, \mathbf{x}, k), \boldsymbol{\Sigma}_\theta(\mathbf{y}_k, \mathbf{x}, k)) \end{aligned} \quad (13)$$

Similarly, variational inference is used to maximize $\log p_\theta(\mathbf{y}_0 | \mathbf{x})$, and the evidence lower bound is computed as:

$$ELBO = \mathbb{E}_q \log p(\mathbf{y}_K | \mathbf{x}) + \mathbb{E}_q \sum_{k=1}^K \log \frac{p_\theta(\mathbf{y}_{k-1} | \mathbf{y}_k, \mathbf{x})}{q(\mathbf{y}_k | \mathbf{y}_{k-1})} \quad (14)$$

If we choose a large step K , then the first term can also be ignored like DDPM because:

$$\log p(\mathbf{y}_K | \mathbf{x}) = \log \mathbb{E}_{p(\mathbf{y}_0 | \mathbf{x})} q(\mathbf{y}_K | \mathbf{y}_0) \quad (15)$$

where $q(\mathbf{y}_K | \mathbf{y}_0)$ is always a normal distribution. This is what [32] does. The final loss function will be:

$$L(\theta) = \mathbb{E}_q \|\epsilon - \epsilon_\theta(\mathbf{y}_k, x, k)\|^2 \quad (16)$$

where the noised added in the k -th step will be predicted under the guidance of the context vector.

To implement the aforementioned process, it is crucial to ensure that $q(\mathbf{y}_K | \mathbf{y}_0)$ is always a normal distribution under any context vector. This requirement usually necessitates a large number of diffusion steps, which can be inefficient and time-consuming for inference. Additionally, when dealing with complex original distributions, determining the appropriate number of steps for completing the diffusion process is difficult. Therefore, in the following section, we present our solution which aims to generate multimodal trajectory distributions more efficiently.

IV. MODEL DESCRIPTION

This section starts with a concise overview of IDM's architecture. We subsequently delve into more comprehensive explanations of the diffusion processes for goals and trajectories. Finally, we present implementation details.

A. Architecture

The overall architecture of IDM is presented in Fig 3. We follow an encoder-decoder architecture. The encoder takes all observations as inputs and produces a context vector, referred to as the "context" for simplicity. The decoder then transforms this context into multiple future trajectories. In this paper, we focus on designing the decoder, making the model independent of the specific encoder used. The decoder consists of two diffusion processes: 1) Goal Diffusion Process: This process aims to model the uncertainty associated with the goal (endpoint). The denoising function in the reverse process is parameterized by an EndNet. 2) Trajectory Diffusion Process: This process models the uncertainty of action given a specific goal. To expedite the diffusion process, we develop a PriorNet that estimates the prior noise distribution. Furthermore, we discover that the goal itself can provide clues for the estimation of the prior noise distribution. With the prior noise distribution established, we employ a PathNet to iteratively eliminate noise and generate the final trajectories.

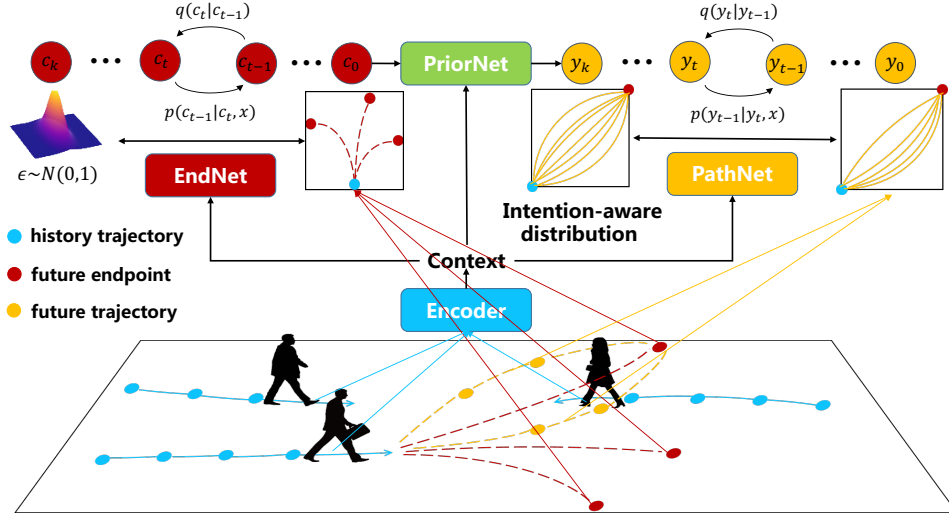


Fig. 3. Overall structure of intention-aware trajectory diffusion model: a) EndNet: It models the diffusion process of the agent’s endpoints. b) PathNet: It models the diffusion process of the agent’s trajectories conditioned on a specific endpoint. c) PriorNet: It estimates the initial noise distribution of the trajectory diffusion process with fewer steps.

B. Goal Diffusion Process

The goal-based diffusion process aims to learn the distribution of endpoints under a specific context. This process is denoted as (c_0, c_1, \dots, c_K) , where K represents the number of diffusion steps, and c_0 represents the ground truth distribution. As the diffusion progresses, c_0 gradually transitions towards a random noise distribution. The forward process is formulated as follows:

$$q(\mathbf{c}_{1:K} | \mathbf{c}_0, \mathbf{x}) := \prod_{k=1}^K q(\mathbf{c}_k | \mathbf{c}_{k-1}) \quad (17)$$

$$q(\mathbf{c}_k | \mathbf{c}_{k-1}) := \mathcal{N}(\mathbf{c}_k; \sqrt{1 - \beta_t} \mathbf{c}_{k-1}, \beta_k \mathbf{I})$$

In our approach, we adopt a large value of K , similar to conventional DDPM. As the diffusion process progresses, c_K can be considered as following a normal distribution. According to Sec. III, the noise injected at each diffusion step is parameterized by a neural network called EndNet, represented as $\epsilon_{\theta}(\mathbf{c}_k, \mathbf{x}, k)$. To generate the eventual endpoints, we follow a step-by-step procedure, utilizing the EndNet-generated noise. More specifically, the endpoints are generated iteratively as follows:

$$\mathbf{c}_{k-1} = \frac{1}{\sqrt{\alpha_k}} \left(\mathbf{c}_k - \frac{\beta_k}{\sqrt{1 - \alpha_k}} \epsilon_{\theta}(\mathbf{c}_k, \mathbf{x}, k) \right) \quad (18)$$

where θ represents the parameters of the EndNet. The loss function for the goal diffusion process is:

$$L_{goal} = \mathbb{E}_q \|\epsilon - \epsilon_{\theta}(\mathbf{c}_k, \mathbf{x}, k)\|^2 \quad (19)$$

In this process, the sample being modeled is a 2-D location, which leads to a significant reduction in inference time.

C. Trajectory Diffusion Process

When the goal is determined, the trajectory of the agent may include uncertainties. For example, a pedestrian may react to the presence of surrounding objects by opting for a

moderate or aggressive action to avoid a collision, as illustrated in Fig. 3. To address these uncertainties, we introduce an additional diffusion process that is specifically designed to incorporate the agent’s intention. This integration of intention into the diffusion process enables more precise predictions of the agent’s future movements.

First, the forward process is defined as:

$$q(\mathbf{y}_{1:S} | \mathbf{y}_0, \mathbf{x}) := \prod_{k=1}^K q(\mathbf{y}_s | \mathbf{y}_{s-1}) \quad (20)$$

$$q(\mathbf{y}_s | \mathbf{y}_{s-1}) := \mathcal{N}(\mathbf{y}_s; \sqrt{1 - \beta_t} \mathbf{y}_{s-1}, \beta_s \mathbf{I})$$

where S is the number of steps and differs from that of goal diffusion K . If S is small, the first term of Eq 14 can not be ignored, because y_S is not a constant normal distribution. The new evidence lower bound is computed as follows:

ELBO

$$\begin{aligned} &= \mathbb{E}_q \log p(\mathbf{y}_S | \mathbf{x}) + \mathbb{E}_q \sum_{s=1}^S \log \frac{p_{\theta}(\mathbf{y}_{s-1} | \mathbf{y}_s, \mathbf{x})}{q(\mathbf{y}_s | \mathbf{y}_{s-1})} \\ &= \mathbb{E}_q \left[\log \frac{p(\mathbf{y}_S | \mathbf{x}) p_{\theta}(\mathbf{y}_0 | \mathbf{y}_1, \mathbf{x})}{q(\mathbf{y}_1 | \mathbf{y}_0)} + \sum_{s=2}^S \frac{p_{\theta}(\mathbf{y}_{s-1} | \mathbf{y}_s, \mathbf{x})}{q(\mathbf{y}_s | \mathbf{y}_{s-1})} \right] \\ &= \mathbb{E}_q \left[\log \frac{p(\mathbf{y}_S | \mathbf{x}) p_{\theta}(\mathbf{y}_0 | \mathbf{y}_1, \mathbf{x})}{q(\mathbf{y}_S | \mathbf{y}_0)} + \sum_{s=2}^S \frac{p_{\theta}(\mathbf{y}_{s-1} | \mathbf{y}_s, \mathbf{x})}{q(\mathbf{y}_{s-1} | \mathbf{y}_s, \mathbf{y}_0)} \right] \\ &= \mathbb{E}_q \log p_{\theta}(\mathbf{y}_0 | \mathbf{y}_1, \mathbf{x}) - D_{KL}(q(\mathbf{y}_S | \mathbf{y}_0) \| p(\mathbf{y}_S | \mathbf{x})) \\ &\quad - \sum_{s=2}^S \mathbb{E}_q [D_{KL}(q(\mathbf{y}_{s-1} | \mathbf{y}_s, \mathbf{y}_0) \| p_{\theta}(\mathbf{y}_{s-1} | \mathbf{y}_s, \mathbf{x}))] \end{aligned} \quad (21)$$

where the sum of the first and third terms equals the EVLB of the original diffusion process. The second term varies only with $p(\mathbf{y}_S | \mathbf{x})$, and a large S leads to an extreme condition where the second term is a constant. Then the loss function

of the trajectory diffusion process is defined according to:

$$L_{traj} = L_{diff} + L_{prior} \quad (22)$$

where L_{diff} is the negative sum of the first and third term, and L_{prior} is the negative of the second term. The computation of L_{diff} is the same as in the conventional diffusion process:

$$L_{diff} = \mathbb{E}_q \|\epsilon - \epsilon_\varphi(\mathbf{y}_s, \mathbf{x}, s)\|^2 \quad (23)$$

where φ denotes the parameters of the network that estimates the noise at each step.

To compute L_{prior} , an intuitive practice is to parameterize the $p(\mathbf{y}_S | x)$ with another neural network represented by ϕ , like what the variational autoencoder does. Considering that $q(\mathbf{y}_S | \mathbf{y}_0)$ is a \mathbf{g} distribution $q(\mathbf{y}_S | \mathbf{y}_0) = \mathcal{N}(\mathbf{y}_S; \sqrt{\bar{\alpha}_S} \mathbf{y}_0, (1 - \bar{\alpha}_S) \mathbf{I})$, according to Eq. 3, we also take $p(\mathbf{y}_S | x)$ as a \mathbf{G} distribution. The neural network estimates the mean $\mu_\phi(x)$ and variance $\sigma_\phi(x)$ of $p(\mathbf{y}_S | x)$. To simplify the computation, we make $\sigma_\phi(x) = (1 - \bar{\alpha}_S) \mathbf{I}$, and compute L_{prior} as follows:

$$L_{prior} = \|\mu_\phi(\mathbf{x}) - \sqrt{\bar{\alpha}_S} \mathbf{y}_0\|^2 \quad (24)$$

In this computation, there is a question about whether a Gaussian distribution is sufficient to capture all the information in $p(\mathbf{y}_S | x)$. Previous study [10] highlights that the trajectory distribution can be decomposed into multiple independent distributions conditioned on the goals of the agent.

$$p(\mathbf{y}_0 | x) = \int p(\mathbf{c} | x) p(\mathbf{y}_0 | x, \mathbf{c}) d\mathbf{c} \quad (25)$$

where \mathbf{c} denotes the goal of the agent. Then $p(\mathbf{y}_S | x)$ is formulated as:

$$\begin{aligned} p(\mathbf{y}_S | x) &= \int p(\mathbf{y}_0 | x) p(\mathbf{y}_S | x, \mathbf{y}_0) d\mathbf{y}_0 \\ &= \iint p(\mathbf{c} | x) p(\mathbf{y}_0 | x, \mathbf{c}) q(\mathbf{y}_S | \mathbf{y}_0) d\mathbf{c} d\mathbf{y}_0 \\ &= \int p(\mathbf{c} | x) p(\mathbf{y}_S | x, \mathbf{c}) d\mathbf{c} \end{aligned} \quad (26)$$

If we decompose the distribution $p(\mathbf{y}_S | x)$ by conditioning on targets, we can calculate L_{prior} as follows:

$$\begin{aligned} L_{prior} &= D_{KL}(q(\mathbf{y}_S | \mathbf{y}_0) \| p(\mathbf{y}_S | x)) \\ &= D_{KL}\left(q(\mathbf{y}_S | \mathbf{y}_0) \left\| \int p(\mathbf{c} | x) p(\mathbf{y}_S | x, \mathbf{c}) d\mathbf{c} \right.\right) \\ &= -\mathbb{E}_{q(\mathbf{y}_S | \mathbf{y}_0)} \log \frac{\mathbb{E}_{p(\mathbf{c} | \mathbf{x})} p(\mathbf{y}_S | x, \mathbf{c})}{q(\mathbf{y}_S | \mathbf{y}_0)} \\ &\leq -\mathbb{E}_{q(\mathbf{y}_S | \mathbf{y}_0)} \mathbb{E}_{p(\mathbf{c} | \mathbf{x})} \log \frac{p(\mathbf{y}_S | x, \mathbf{c})}{q(\mathbf{y}_S | \mathbf{y}_0)} \\ &= \mathbb{E}_{p(\mathbf{c} | \mathbf{x})} D_{KL}(q(\mathbf{y}_S | \mathbf{y}_0) \| p(\mathbf{y}_S | x, \mathbf{c})) \end{aligned} \quad (27)$$

where the upper bound of L_{prior} is induced according to Jensen's inequality. During training, we minimize the upper bound of L_{prior} , which we call L_{prior} latter. Instead of modeling the whole trajectory distribution, we parameterize the distribution of the trajectory conditioned on the goal with a neural network ϕ . The final L_{prior} is calculated by:

$$L_{prior} = \mathbb{E}_{p(\mathbf{c} | \mathbf{x})} \|\mu_\phi(\mathbf{x}, \mathbf{c}) - \sqrt{\bar{\alpha}_S} \mathbf{y}_0\|^2 \quad (28)$$

Compared with $p(\mathbf{y}_S | x)$, $p(\mathbf{y}_S | x, \mathbf{c})$ is more suitable to be modeled as a Gaussian distribution, and could lead to small prior loss. The insight is in accord with previous works [73], [83], which regard the future trajectory as a multimodal distribution. Our experiments verify this point in Sec. V-D.

D. Model details

A model instantiated from our architecture consists of four blocks: Encoder, EndNet, PriorNet, and PathNet, which we will elaborate literally as follows.

1) *Encoder*: Our architecture focuses on the decoder based on the diffusion process and therefore is encoder-agnostic. In this work, we utilize the encoder from a classical model called Trajectron++ [19]. Trajectron++ follows a CVAE framework. The encoder in Trajectron++ incorporates all observations into a hidden embedding, while the decoder transforms the embedding into plenty of future trajectories. It consists of three main blocks: 1) LSTM network modeling the agent history; 2) Aggregation block that encodes agent interactions; 3) CNN based map encoder which represents the semantic maps by a vector. The final output of the encoder is concatenated by the above embeddings. We follow their encoder settings.

2) *EndNet*: EndNet is responsible for parameterizing $\epsilon_\theta(\mathbf{c}_k, x, k)$. It takes x , step k , and the goal at that step \mathbf{c}_k as inputs, and produces the estimated noise. These inputs are concatenated and fed into a Multi-Layer Perceptron (MLP). We evaluate the performance of EndNet with different numbers of layers in Sec. V-D.

3) *PriorNet*: PriorNet is used to model $\mu_\phi(x, \mathbf{c})$, which represents the mean of the prior distribution $p(\mathbf{y}_S | x)$. The inputs include the context vector $x \in \mathbb{R}^D$ and the goal of the agent $\mathbf{c} \in \mathbb{R}^2$. The output of PriorNet is $\mathbf{y}_S \in \mathbb{R}^{T_Q \times 2}$, where T_Q represents the number of future time steps. There could exist temporal correlations among future trajectories. Therefore, we generate the prior distribution based on a neural network that captures temporal correlation. MLP, RNN, TCN, and Transformer are all validated in our experiments.

4) *PathNet*: PathNet tries to parameterize the $\epsilon_\varphi(\mathbf{y}_s, x, s)$. The network takes $\mathbf{y}_s \in \mathbb{R}^{T_Q \times 2}$, $x \in \mathbb{R}^D$ and s as inputs and produces the estimated noise $\epsilon \in \mathbb{R}^{T_Q \times 2}$. To utilize the temporal correlation, we also develop several versions of PathNet based on MLP, RNN, TCN, and Transformer.

E. Training and Inference

1) *Training*: During training, we know both the historical observations and future trajectories. The training loss is defined by:

$$L_{total} = L_{goal} + \lambda_1 L_{diff} + \lambda_2 L_{prior} \quad (29)$$

where L_{goal} and L_{diff} are calculated according to Eq. 19 and Eq. 23. λ_1 and λ_2 control the importance of the loss for the trajectory diffusion process and loss for prior distribution estimation, respectively. Because \mathbf{c}_k is sampled from a Gaussian distribution based on \mathbf{c}_0 according to Eq. 3, which is non-differentiable during training, we apply the reparameterization

trick. Specifically, we get a sample ϵ from normal distribution, and obtain \mathbf{c}_k by:

$$\mathbf{c}_k = \sqrt{\bar{\alpha}_k} \mathbf{c}_0 + (1 - \bar{\alpha}_k) \epsilon \quad (30)$$

\mathbf{y}_s in L_{diff} is acquired by the same way.

Similar to previous works [10], we acquire L_{prior} by a teacher-forcing manner, where the realistic goal \mathbf{c}_0 is used to guide the calculation:

$$L_{prior} = \|\mu_\phi(x, \mathbf{c}_0) - \sqrt{\bar{\alpha}_S} \mathbf{y}_0\|^2 \quad (31)$$

The complete training procedure is shown in Algorithm 1.

Algorithm 1 Training

Input: $x, e, \mathcal{M}, y; \alpha_{1:K}^g, \alpha_{1:S}^t; \lambda_1, \lambda_2$

Output: Encoder g_ψ , EndNet ϵ_θ , PriorNet μ_ϕ , PathNet ϵ_φ
repeat

 Compute context vector $\mathbf{x} = g_\psi(x, e, \mathcal{M})$

$\mathbf{y}_0 = y, \mathbf{c}_0 = y[-1]$

$k \sim \text{Uniform}(\{1, 2, \dots, K\}), s \sim \text{Uniform}(\{1, 2, \dots, S\})$

$\epsilon \sim \mathcal{N}(\mathbf{0}, \mathbf{I})$

$\mathbf{c}_k = \sqrt{\bar{\alpha}_k^g} \mathbf{c}_0 + (1 - \bar{\alpha}_k^g) \epsilon$

$\mathbf{y}_s = \sqrt{\bar{\alpha}_s^t} \mathbf{y}_0 + (1 - \bar{\alpha}_s^t) \epsilon$

 Compute $L_{goal}, L_{diff}, L_{prior}$ according to Eq. 19,23,31

 Take gradient descent step on

$\nabla_{\psi, \theta, \varphi, \phi}(L_{goal} + \lambda_1 L_{diff} + \lambda_2 L_{prior})$

until converged

2) *Inference:* In the inference phase, we aim to generate \mathcal{K} plausible predictions. The goal is predicted by the iterative diffusion process first, and is then utilized to initialize \mathbf{y}_S . Finally, the trajectory conditioned on the goal is generated by another diffusion process with fewer steps. The details are described in Algorithm 2.

Algorithm 2 Inference

Input: $x, e, \mathcal{M}, y; \alpha_{1:K}^g, \alpha_{1:S}^t, g_\psi, \epsilon_\theta, \mu_\phi, \epsilon_\varphi$

Output: $\{y_i \in \mathbb{R}^{T_Q \times 2} \mid i = 1, 2, \dots, \mathcal{K}\}$

Compute context vector $\mathbf{x} = g_\psi(x, e, \mathcal{M})$

for $i = 1, \dots, \mathcal{K}$ **do**

$\mathbf{c}_K \sim \mathcal{N}(\mathbf{0}, \mathbf{I})$

for $k = K, \dots, 1$ **do**

$\mathbf{c}_{k-1} = \frac{1}{\sqrt{\alpha_k^g}} \left(\mathbf{c}_k - \frac{\beta_k^g}{\sqrt{1 - \bar{\alpha}_k^g}} \epsilon_\theta(\mathbf{c}_k, \mathbf{x}, k) \right)$

end for

$\epsilon \sim \mathcal{N}(\mathbf{0}, \mathbf{I})$

$\mathbf{y}_S = \mu_\phi(\mathbf{x}, \mathbf{c}_0) + (1 - \bar{\alpha}_S) \epsilon$

for $s = S, \dots, 1$ **do**

$\mathbf{y}_{s-1} = \frac{1}{\sqrt{\alpha_s^t}} \left(\mathbf{y}_s - \frac{\beta_s^t}{\sqrt{1 - \bar{\alpha}_s^t}} \epsilon_\varphi(\mathbf{y}_s, \mathbf{x}, s) \right)$

end for

$y_i = \mathbf{y}_0$

end for

return $\{y_i \in \mathbb{R}^{T_Q \times 2} \mid i = 1, 2, \dots, \mathcal{K}\}$

V. EXPERIMENTS

A. Experiment Setup

1) *Dataset:* We use Stanford Drone Datasets (SDD) and UCY/ETH to evaluate our methods.

SDD: It is a large-scale dataset aimed at trajectory prediction. The data is collected by a drone from a bird’s-eye view perspective. It contains 60 recordings referring to 20 scenes around a university campus and describes the movements of multiple pedestrians and vehicles. The trajectory data is sampled at 2.5 FPS. Following previous works [71], we conduct experiments on 47 recordings about pedestrian trajectory, with 30 of them used as training data, while the remaining 17 recordings are used to test the model’s performance.

ETH/UCY: The dataset is a classical benchmark for pedestrian trajectory prediction. The data comes from the surveillance video on the street. The dataset comprises five scenes, namely, ETH, Hotel, UNIV, ZARA1, and ZARA2. The sampling frequency is 2.5 FPS. We adopt the leave-one-scene-out setting like [13], where 4 scenes are used for training and the remaining scene is used for testing.

TABLE II
PERFORMANCE ON SDD DATASET

Methods	Decoder	U_{goal}	U_{traj}	ADE	FDE
Social-LSTM	BG	-	✓	57.00	31.20
Expert+GMM	BG	-	✓	10.67	14.38
SimAug	Grid	✓	-	10.27	19.71
PCCSNET	Grid	✓	-	8.62	16.16
Y-Net	Grid	✓	✓	8.97	14.61
Social-GAN	GAN	-	✓	27.23	41.44
Goal-GAN	GAN	✓	-	12.20	22.10
MG-GAN	GAN	-	✓	13.60	25.80
CGNS	CVAE	-	✓	15.60	28.20
Trajectron++	CVAE	-	✓	8.98	19.02
PECNET	CVAE	✓	-	9.96	15.88
LB-EBM	Energy	✓	✓	8.87	15.61
MID	Diffusion	-	✓	7.61	14.30
IDM	Diffusion	✓	✓	7.46	13.83

2) *Metrics:* To evaluate the effectiveness of our model, ADE and FDE are used to measure the accuracy of predictions. Average Displacement Error (ADE) represents the average point-to-point Euclidean distance between the predicted trajectory and the ground truth. Final Displacement Error (FDE) describes the error between the predicted endpoint and the realistic endpoint. The error is measured by pixel in SDD and by meter in ETH/UCY. Given multiple predictions, the best-of-N strategy [13] is utilized to compute the final metric.

3) *Implementation Details:* During the training stage, the batch size is set to 256, the learning rate is set to 0.0001, λ_1 is set to 1, and λ_2 is set to 0.5. All experiments are conducted on a single RTX 3090. During the prediction stage, we generate 20 predictions for each agent and calculate the minimum ADE/FDE based on these predictions. For each dataset, we repeat the evaluation five times and report the average results.

B. Comparison with SOTA methods

The results for the SDD dataset are presented in Table II. The table includes all the methods along with their decoder type and whether they model the uncertainty of the goal

TABLE III
PERFORMANCE ON ETH/UCY DATASETS

Methods	Deocoder	Sample	ETH		HOTEL		UNIV		ZARA1		ZARA2		AVG	
			ADE	FDE	ADE	FDE	ADE	FDE	ADE	FDE	ADE	FDE	ADE	FDE
Social-LSTM	BG	20	1.09	2.35	0.79	1.76	0.67	1.40	0.47	1.00	0.56	1.17	0.72	1.54
Social-STGCN	BG	20	0.64	1.11	0.49	0.85	0.44	0.79	0.34	0.53	0.30	0.48	0.44	0.75
Causal-STGCN	BG	20	0.64	1.00	0.38	0.45	0.49	0.81	0.34	0.53	0.32	0.49	0.43	0.66
STAR	BG	20	0.36	0.65	0.17	0.36	0.31	0.62	0.26	0.55	0.22	0.46	0.26	0.53
Expert-GMM	BG	20	0.37	0.65	0.11	0.15	0.20	0.44	0.15	0.31	0.12	0.26	0.19	0.36
PCCSNET	Grid	20	0.28	0.54	0.11	0.19	0.29	0.60	0.21	0.44	0.15	0.34	0.21	0.42
Social-GAN	GAN	20	0.81	1.52	0.72	1.61	0.60	1.26	0.34	0.69	0.42	0.84	0.58	1.18
Goal-GAN	GAN	20	0.59	1.18	0.19	0.35	0.60	1.19	0.43	0.87	0.32	0.65	0.43	0.85
Social-BIGAT	GAN	20	0.69	1.29	0.49	1.01	0.55	1.32	0.30	0.62	0.36	0.75	0.48	1.00
MG-GAN	GAN	20	0.47	0.91	0.14	0.24	0.54	1.07	0.36	0.73	0.29	0.60	0.36	0.71
CGNS	CVAE	20	0.62	1.40	0.70	0.93	0.48	1.22	0.32	0.59	0.35	0.71	0.49	0.97
PECNET	CVAE	20	0.54	0.87	0.18	0.24	0.35	0.60	0.22	0.39	0.17	0.30	0.29	0.48
Trajectron++	CVAE	20	0.39	0.83	0.12	0.21	0.20	0.44	0.15	0.33	0.11	0.25	0.19	0.41
LB-EBM	Energy	20	0.30	0.52	0.13	0.20	0.27	0.52	0.20	0.37	0.15	0.29	0.21	0.38
MID	Diffusion	20	0.39	0.66	0.13	0.22	0.22	0.45	0.17	0.30	0.13	0.27	0.21	0.38
IDM	Diffusion	20	0.41	0.62	0.15	0.25	0.20	0.42	0.17	0.28	0.12	0.25	0.21	0.36

and trajectory. The Bivariate Gaussian (BG) models assume that future positions follow a bivariate Gaussian distribution and utilize maximum likelihood estimation to compute the parameters of the distribution. The methods make strong assumptions about the trajectory distribution, which can result in a poor fit to real data. The grid-based models divide the scene into grid cells and predict the occupancy probability of each cell in the future. While these methods achieve outstanding performance, they require significant effort to construct and train the trajectory map [23]. Generative models like GAN and CVAE are also used to generate future trajectories. However, training GAN-based models can be uncontrollable [16], while the CVAE-based models tend to generate unnatural trajectories [32]. Overall, our method achieves the best performance among all existing methods in both metrics, with an ADE of 7.46 and an FDE of 13.83 in pixel coordinates. In addition, two findings can be acquired from the results. First, MID and IDM perform better than all other kinds of methods, demonstrating that diffusion models have great potential in trajectory prediction. Second, our model also outperforms MID. This is because MID does not consider the uncertainty of the goal, and can therefore lose accuracy, especially in long-term prediction. Our model reduces the FDE by 0.47 compared to MID. Hence, it is essential to model the uncertainty of agents' intentions and trajectories.

Table III presents the results on ETH/UCY dataset. The prediction results of IDM are comparable to those of existing methods, with an average ADE of 0.21 and FDE of 0.36. While IDM may not improve the MID in all datasets, it achieves similar performance with less time and memory requirement, as demonstrated in Sec. V-E. Furthermore, compared to MID, our method can generate more natural trajectories, as shown in Sec. V-C.

C. Visualization

In order to investigate the diversity and accuracy of our model, we generate 20 predictions using both our model and MID on all datasets and visualize the predictions. Fig. 4 and Fig. 5 display the results on SDD and ETH/UCY, respectively. The black dashed line represents the historical trajectory, the

white dashed line represents the ground truth future trajectory, and the blue solid line represents the predicted trajectory. Both MID and IDM generate diverse predictions, including some that closely approach the ground truth future trajectories. However, MID tends to produce some unnatural trajectories. For example, on SDD datasets, a pedestrian is predicted to turn around in the first case and abruptly steer in the third case. Additionally, the predictions generated by MID sometimes appear uneven as seen in the sixth case where a pedestrian is expected to follow a twisted trajectory. Similar results have been observed in predictions on ETH/UCY datasets. In contrast, IDM tends to generate smoother and more realistic trajectories that resemble plausible future movements.

To quantify these differences, we reduce the number of predictions and observe the minimum ADE and FDE of the two methods. The results are presented in Table IV. Our method consistently outperformed MID in both metrics, regardless of the number of predictions made. Furthermore, the superiority of our method becomes more distinct as the number of samples decreases. This is because MID is more prone to predicting unnatural trajectories that deviate significantly from the ground truth. When making fewer predictions, there is a higher likelihood those correct and natural predictions may be excluded. Our model mitigates this problem by incorporating the predicted goals into the generation of trajectories.

We also present the predicted trajectory distribution of MID and our method as contours in Fig. 6. It can be observed that, compared with MID, our method predicts a smaller walkable region, indicating that more implausible trajectories can be excluded. Furthermore, the uncertainty of the trajectory predicted by our method increases with the prediction step, which aligns with our intuition. In contrast, the predictions of MID present high uncertainty even though in the early future. Additionally, as shown in the fourth case, MID may generate unnatural distributions where pedestrians have a higher chance of turning around. Overall, by introducing intention information, our method enables predictions that better fit the real distribution.



Fig. 4. Prediction on SDD

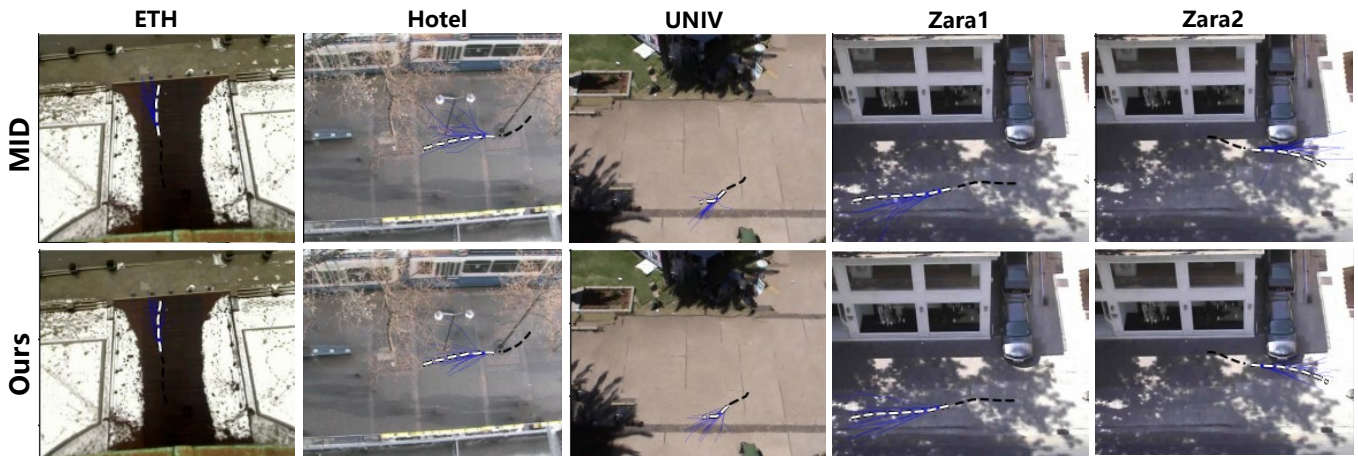


Fig. 5. Prediction on ETH/UCY

TABLE IV
ADE/FDE UNDER DIFFERENT NUMBER OF PREDICTIONS

	4	8	12	16	20
MID	12.40/27.45	10.11/21.30	9.09/19.27	8.48/16.42	7.61/14.30
Ours	11.19/24.58	9.44/19.74	8.38/17.79	7.85/15.80	7.46/13.83

D. Ablation Study

In this section, we begin by analyzing the role of each component in our architecture. Next, we validate the selection of each component. Finally, we evaluate the impact of the step number on the prediction results.

Table V presents the prediction results when each component is absent. First, the variants without the PriorNet apply fewer steps in the diffusion process and still consider initial signals as Gaussian noise. During the training process, it does not consider the prior loss in Eq. 28. This variant exhibits

the highest prediction error in both ADE and FDE. This highlights the importance of estimating the initial distribution for the diffusion process with fewer steps. The second variant only models the distribution of the goal and uses MLP to generate trajectories conditioned on the given goal. The variant achieves a higher ADE and FDE because it ignores the action uncertainty, which can be modeled by another diffusion process. The third variant models the action uncertainty with the trajectory diffusion process. However, the estimation of the prior distribution solely relies on the context vector and does not take into account any information about the goal. Our model surpasses it by 6.8% in ADE and 10.3% in FDE. This demonstrates that incorporating goal information can provide crucial cues for accurately estimating the prior distribution of the diffusion process.

To make the most of our model’s efficacy, we explore different selections for each component. Fig. 7(a) shows the

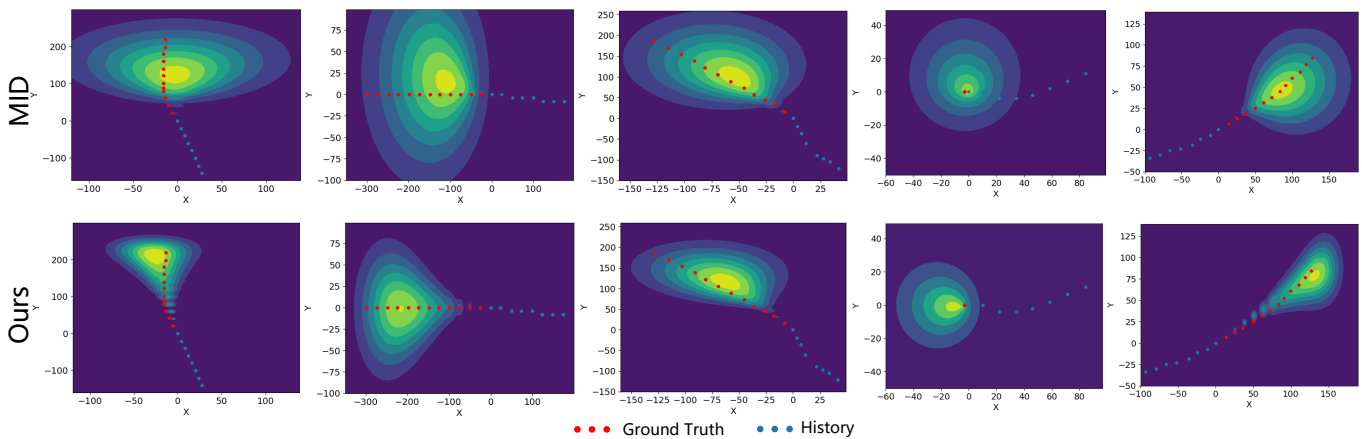


Fig. 6. Counter map of predictions

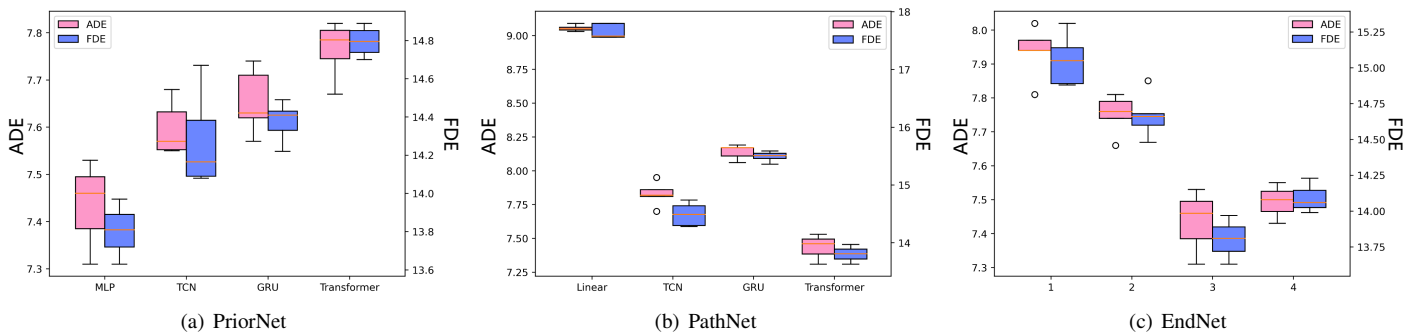


Fig. 7. Selection of each component

performance of different PriorNet. Surprisingly, the MLP selection achieves the best performance. This suggests that, given a fixed goal, the most probable prior trajectory distribution is simple, and complex networks are more susceptible to overfitting. For PathNet, we try similar networks, but find that the complex Transformer performs better than other choices (Fig. 7(b)). It indicates that Transformer excels at modeling the uncertainty of trajectories that exhibit temporal correlation. We also experiment with different layers in the MLP for EndNet and find that three is the most suitable number (Fig. 7(c)). Increasing the number of layers does not result in improved performance.

Furthermore, we discuss the influence of step numbers on the model. Fig. 9 shows the performance under different steps of the goal and trajectory diffusion process. Firstly, increasing the number of steps in the goal diffusion process results in more precise predictions, because accurate goal prediction helps in estimating the prior distribution in the trajectory diffusion process. Secondly, given the specific goal, the prediction result is not susceptible to the number of steps in the trajectory diffusion process. This is because our PriorNet can predict the suitable prior distribution for different steps. The best result, as reported above, is achieved when the goal and trajectory steps are set to 100 and 10, respectively.

TABLE V
PERFORMANCE INFLUENCED BY EACH COMPONENT

EndNet	PriorNet	PathNet	ADE	FDE
✓	—	✓	9.40	17.34
✓	—	—	7.85	15.44
—	✓	✓	7.98	15.41
✓	✓	✓	7.46	13.83

E. Efficiency

We compare the inference speed of our model with that of the conventional diffusion model. Fig. 8(a) demonstrates the execution time per prediction of the two methods on different datasets. Compared to MID, our method experiences nearly a threefold decrease in inference time. This superiority stems from two reasons. Firstly, our goal diffusion process handles 2-D locations, whereas MID handles sequences. Secondly, our model completes the trajectory diffusion process in just one-tenth of the steps. Additionally, in the scenes with high population density, the inference time further increases. Across all datasets, our method achieves a prediction in less than 240ms. Fig. 8(b) illustrates the inference time of our model with different steps of the goal and trajectory diffusion process. As the number of steps increases, the inference time demonstrates an approximately linear increase. Moreover, when comparing the same number of steps, goal diffusion requires significantly less time than the trajectory diffusion process, indicating that reducing the target dimension is effective in shortening the

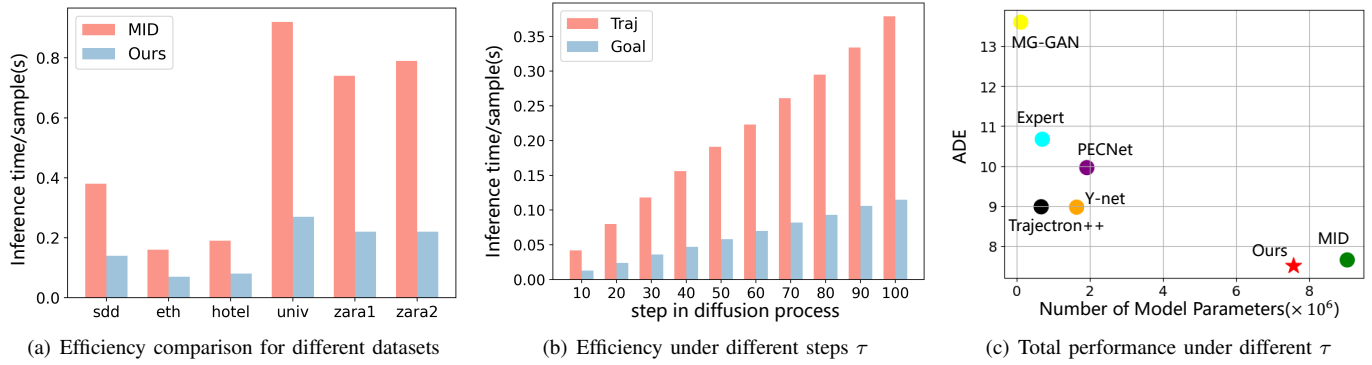


Fig. 8. Inference time and model parameter

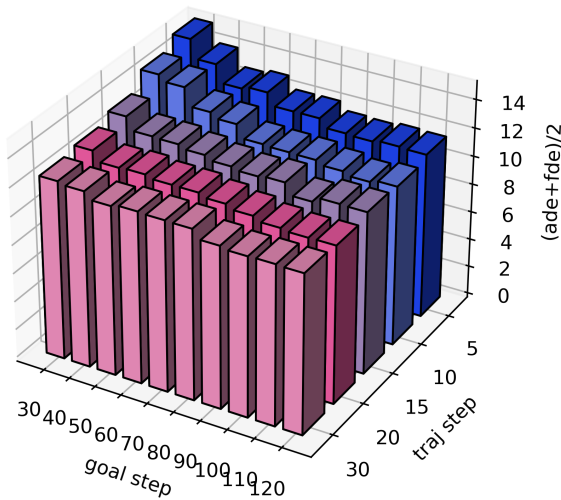


Fig. 9. Selection of diffusion steps for goal and trajectory

time.

Furthermore, we also summarize the model parameters of our model. As shown in Fig. 8(c), our model reduces the parameters by one-fifth compared to the original MID. However, the superiority of the diffusion model in trajectory prediction comes at the expense of more model parameters. In the future, we plan to propose the development of a lightweight diffusion model for trajectory prediction.

VI. CONCLUSION

In this work, we design an intention-aware diffusion model for multimodal trajectory prediction. The uncertainty of trajectories is decoupled into goal uncertainty and action uncertainty, and is modeled by two interconnected diffusion processes. To improve the efficiency of the inference process, instead of assuming a normal prior noise distribution, we devise a PriorNet to estimate the specific prior distribution of the diffusion process, thus reducing the required number of steps for a complete diffusion process. Additionally, we augment the original loss function by incorporating the estimation error of the prior distribution. We conduct experiments on two real-world datasets, SDD and ETH/UCY. Our method achieves state-of-the-art results. Compared to the original diffusion

model, our approach reduces the inference time by two-thirds. Furthermore, our experiments reveal the benefits of introducing intention information in modeling the diffusion process with fewer steps.

REFERENCES

- [1] Y. Huang, J. Du, Z. Yang, Z. Zhou, L. Zhang, and H. Chen, "A survey on trajectory-prediction methods for autonomous driving," *IEEE Transactions on Intelligent Vehicles*, vol. 7, no. 3, pp. 652–674, 2022.
- [2] W. Zhu, Y. Liu, M. Zhang, and Y. Yi, "Reciprocal consistency prediction network for multi-step human trajectory prediction," *IEEE Transactions on Intelligent Transportation Systems*, 2023.
- [3] X. Wang, J. Alonso-Mora, and M. Wang, "Probabilistic risk metric for highway driving leveraging multi-modal trajectory predictions," *IEEE Transactions on Intelligent Transportation Systems*, vol. 23, no. 10, pp. 19399–19412, 2022.
- [4] A. Rudenko, L. Palmieri, M. Herman, K. M. Kitani, D. M. Gavrila, and K. O. Arras, "Human motion trajectory prediction: A survey," *The International Journal of Robotics Research*, vol. 39, no. 8, pp. 895–935, 2020.
- [5] H. Hu, Q. Wang, M. Cheng, and Z. Gao, "Trajectory prediction neural network and model interpretation based on temporal pattern attention," *IEEE Transactions on Intelligent Transportation Systems*, vol. 24, no. 3, pp. 2746–2759, 2022.
- [6] D. Helbing and P. Molnar, "Social force model for pedestrian dynamics," *Physical review E*, vol. 51, no. 5, p. 4282, 1995.
- [7] H. Xue, D. Q. Huynh, and M. Reynolds, "Ss-lstm: A hierarchical lstm model for pedestrian trajectory prediction," in *2018 IEEE Winter Conference on Applications of Computer Vision (WACV)*, pp. 1186–1194, IEEE, 2018.
- [8] E. Wang, H. Cui, S. Yalamanchi, M. Moorthy, and N. Djuric, "Improving movement predictions of traffic actors in bird’s-eye view models using gans and differentiable trajectory rasterization," in *Proceedings of the 26th ACM SIGKDD International Conference on Knowledge Discovery & Data Mining*, pp. 2340–2348, 2020.
- [9] J. Gao, C. Sun, H. Zhao, Y. Shen, D. Anguelov, C. Li, and C. Schmid, "Vectormet: Encoding hd maps and agent dynamics from vectorized representation," in *Proceedings of the IEEE/CVF Conference on Computer Vision and Pattern Recognition*, pp. 11525–11533, 2020.
- [10] H. Zhao, J. Gao, T. Lan, C. Sun, B. Sapp, B. Varadarajan, Y. Shen, Y. Shen, Y. Chai, C. Schmid, *et al.*, "Tnt: Target-driven trajectory prediction," in *Conference on Robot Learning*, pp. 895–904, PMLR, 2021.
- [11] V. Trentin, A. Artuñedo, J. Godoy, and J. Villagra, "Multi-modal interaction-aware motion prediction at unsignalized intersections," *IEEE Transactions on Intelligent Vehicles*, 2023.
- [12] R. Huang, H. Xue, M. Pagnucco, F. Salim, and Y. Song, "Multimodal trajectory prediction: A survey," *arXiv preprint arXiv:2302.10463*, 2023.
- [13] A. Gupta, J. Johnson, L. Fei-Fei, S. Savarese, and A. Alahi, "Social gan: Socially acceptable trajectories with generative adversarial networks," in *Proceedings of the IEEE conference on computer vision and pattern recognition*, pp. 2255–2264, 2018.
- [14] L. A. Thiede and P. P. Brahma, "Analyzing the variety loss in the context of probabilistic trajectory prediction," in *Proceedings of the IEEE/CVF International Conference on Computer Vision*, pp. 9954–9963, 2019.

- [15] N. Deo, E. Wolff, and O. Beijbom, "Multimodal trajectory prediction conditioned on lane-graph traversals," in *Conference on Robot Learning*, pp. 203–212, PMLR, 2022.
- [16] K. Guo, W. Liu, and J. Pan, "End-to-end trajectory distribution prediction based on occupancy grid maps," in *Proceedings of the IEEE/CVF Conference on Computer Vision and Pattern Recognition*, pp. 2242–2251, 2022.
- [17] A. Alahi, K. Goel, V. Ramanathan, A. Robicquet, L. Fei-Fei, and S. Savarese, "Social lstm: Human trajectory prediction in crowded spaces," in *Proceedings of the IEEE conference on computer vision and pattern recognition*, pp. 961–971, 2016.
- [18] A. Mohamed, K. Qian, M. Elhoseiny, and C. Claudel, "Social-stgcn: A social spatio-temporal graph convolutional neural network for human trajectory prediction," in *Proceedings of the IEEE/CVF conference on computer vision and pattern recognition*, pp. 14424–14432, 2020.
- [19] T. Salzmann, B. Ivanovic, P. Chakravarty, and M. Pavone, "Trajectron++: Dynamically-feasible trajectory forecasting with heterogeneous data," in *Computer Vision—ECCV 2020: 16th European Conference, Glasgow, UK, August 23–28, 2020, Proceedings, Part XVIII 16*, pp. 683–700, Springer, 2020.
- [20] H. Ben-Younes, E. Zablocki, M. Chen, P. Pérez, and M. Cord, "Raising context awareness in motion forecasting," in *Proceedings of the IEEE/CVF Conference on Computer Vision and Pattern Recognition*, pp. 4409–4418, 2022.
- [21] Y. Liu, Q. Yan, and A. Alahi, "Social nce: Contrastive learning of socially-aware motion representations," in *Proceedings of the IEEE/CVF International Conference on Computer Vision*, pp. 15118–15129, 2021.
- [22] G. Chen, J. Li, N. Zhou, L. Ren, and J. Lu, "Personalized trajectory prediction via distribution discrimination," in *Proceedings of the IEEE/CVF International Conference on Computer Vision*, pp. 15580–15589, 2021.
- [23] K. Mangalam, Y. An, H. Girase, and J. Malik, "From goals, waypoints & paths to long term human trajectory forecasting," in *Proceedings of the IEEE/CVF International Conference on Computer Vision*, pp. 15233–15242, 2021.
- [24] P. Dendorfer, S. Elflein, and L. Leal-Taixé, "Mg-gan: A multi-generator model preventing out-of-distribution samples in pedestrian trajectory prediction," in *Proceedings of the IEEE/CVF International Conference on Computer Vision*, pp. 13158–13167, 2021.
- [25] L. Fang, Q. Jiang, J. Shi, and B. Zhou, "Tpnet: Trajectory proposal network for motion prediction," in *Proceedings of the IEEE/CVF Conference on Computer Vision and Pattern Recognition*, pp. 6797–6806, 2020.
- [26] V. Kosaraju, A. Sadeghian, R. Martín-Martín, I. Reid, H. Rezatofighi, and S. Savarese, "Social-bigat: Multimodal trajectory forecasting using bicycle-gan and graph attention networks," *Advances in Neural Information Processing Systems*, vol. 32, 2019.
- [27] R. Liang, Y. Li, J. Zhou, and X. Li, "Stglow: A flow-based generative framework with dual graphormer for pedestrian trajectory prediction," *arXiv preprint arXiv:2211.11220*, 2022.
- [28] J. Choi, S. Kim, Y. Jeong, Y. Gwon, and S. Yoon, "Ilvr: Conditioning method for denoising diffusion probabilistic models," *arXiv preprint arXiv:2108.02938*, 2021.
- [29] P. Dhariwal and A. Nichol, "Diffusion models beat gans on image synthesis," *Advances in Neural Information Processing Systems*, vol. 34, pp. 8780–8794, 2021.
- [30] A. Q. Nichol and P. Dhariwal, "Improved denoising diffusion probabilistic models," in *International Conference on Machine Learning*, pp. 8162–8171, PMLR, 2021.
- [31] J. Ho and S. Ermon, "Generative adversarial imitation learning," *Advances in neural information processing systems*, vol. 29, 2016.
- [32] T. Gu, G. Chen, J. Li, C. Lin, Y. Rao, J. Zhou, and J. Lu, "Stochastic trajectory prediction via motion indeterminacy diffusion," in *Proceedings of the IEEE/CVF Conference on Computer Vision and Pattern Recognition*, pp. 17113–17122, 2022.
- [33] J. Ho, T. Salimans, A. Gritsenko, W. Chan, M. Norouzi, and D. J. Fleet, "Video diffusion models," *arXiv preprint arXiv:2204.03458*, 2022.
- [34] W. Harvey, S. Naderiparizi, V. Masrani, C. Weilbach, and F. Wood, "Flexible diffusion modeling of long videos," *arXiv preprint arXiv:2205.11495*, 2022.
- [35] N. Chen, Y. Zhang, H. Zen, R. J. Weiss, M. Norouzi, and W. Chan, "Wavegrad: Estimating gradients for waveform generation," *arXiv preprint arXiv:2009.00713*, 2020.
- [36] Z. Kong, W. Ping, J. Huang, K. Zhao, and B. Catanzaro, "Diffwave: A versatile diffusion model for audio synthesis," *arXiv preprint arXiv:2009.09761*, 2020.
- [37] C. Meng, Y. He, Y. Song, J. Song, J. Wu, J.-Y. Zhu, and S. Ermon, "Sdedit: Guided image synthesis and editing with stochastic differential equations," in *International Conference on Learning Representations*, 2021.
- [38] R. Rombach, A. Blattmann, D. Lorenz, P. Esser, and B. Ommer, "High-resolution image synthesis with latent diffusion models," in *Proceedings of the IEEE/CVF Conference on Computer Vision and Pattern Recognition*, pp. 10684–10695, 2022.
- [39] A. Elnagar and K. Gupta, "Motion prediction of moving objects based on autoregressive model," *IEEE Transactions on Systems, Man, and Cybernetics-Part A: Systems and Humans*, vol. 28, no. 6, pp. 803–810, 1998.
- [40] A. Barth and U. Franke, "Where will the oncoming vehicle be the next second?," in *2008 IEEE Intelligent Vehicles Symposium*, pp. 1068–1073, IEEE, 2008.
- [41] Y. Cai, N. de Freitas, and J. J. Little, "Robust visual tracking for multiple targets," in *Computer Vision—ECCV 2006: 9th European Conference on Computer Vision, Graz, Austria, May 7-13, 2006, Proceedings, Part IV 9*, pp. 107–118, Springer, 2006.
- [42] A. Elnagar, "Prediction of moving objects in dynamic environments using kalman filters," in *Proceedings 2001 IEEE International Symposium on Computational Intelligence in Robotics and Automation (Cat. No. 01EX515)*, pp. 414–419, IEEE, 2001.
- [43] R. Schubert, E. Richter, and G. Wanielik, "Comparison and evaluation of advanced motion models for vehicle tracking," in *2008 11th international conference on information fusion*, pp. 1–6, IEEE, 2008.
- [44] A. Møgelmoose, M. M. Trivedi, and T. B. Moeslund, "Trajectory analysis and prediction for improved pedestrian safety: Integrated framework and evaluations," in *2015 IEEE intelligent vehicles symposium (IV)*, pp. 330–335, IEEE, 2015.
- [45] C. Yang, M. Bakich, and E. Blasch, "Nonlinear constrained tracking of targets on roads," in *2005 7th International Conference on Information Fusion*, vol. 1, pp. 8–pp, IEEE, 2005.
- [46] I. Batkovic, M. Zanon, N. Lubbe, and P. Falcone, "A computationally efficient model for pedestrian motion prediction," in *2018 European control conference (ECC)*, pp. 374–379, IEEE, 2018.
- [47] D. Petrich, T. Dang, D. Kasper, G. Breuel, and C. Stiller, "Map-based long term motion prediction for vehicles in traffic environments," in *16th International IEEE Conference on Intelligent Transportation Systems (ITSC 2013)*, pp. 2166–2172, IEEE, 2013.
- [48] X. Yan, I. A. Kakadiaris, and S. K. Shah, "Modeling local behavior for predicting social interactions towards human tracking," *Pattern Recognition*, vol. 47, no. 4, pp. 1626–1641, 2014.
- [49] I. Karamouzas, P. Heil, P. Van Beek, and M. H. Overmars, "A predictive collision avoidance model for pedestrian simulation," in *Motion in Games: Second International Workshop, MIG 2009, Zeist, The Netherlands, November 21-24, 2009, Proceedings 2*, pp. 41–52, Springer, 2009.
- [50] F. Zanlungo, T. Ikeda, and T. Kanda, "Social force model with explicit collision prediction," *Europhysics Letters*, vol. 93, no. 6, p. 68005, 2011.
- [51] H. Gong, J. Sim, M. Likhachev, and J. Shi, "Multi-hypothesis motion planning for visual object tracking," in *2011 International Conference on Computer Vision*, pp. 619–626, IEEE, 2011.
- [52] M. Bahram, A. Lawitzky, J. Friedrichs, M. Aeberhard, and D. Wollherr, "A game-theoretic approach to replanning-aware interactive scene prediction and planning," *IEEE Transactions on Vehicular Technology*, vol. 65, no. 6, pp. 3981–3992, 2015.
- [53] Y. F. Chen, M. Liu, M. Everett, and J. P. How, "Decentralized non-communicating multiagent collision avoidance with deep reinforcement learning," in *2017 IEEE international conference on robotics and automation (ICRA)*, pp. 285–292, IEEE, 2017.
- [54] C. Rösmann, F. Hoffmann, and T. Bertram, "Timed-elastic-bands for time-optimal point-to-point nonlinear model predictive control," in *2015 European control conference (ECC)*, pp. 3352–3357, IEEE, 2015.
- [55] F. Previtali, A. Bordallo, L. Iocchi, and S. Ramamoorthy, "Predicting future agent motions for dynamic environments," in *2016 15th IEEE International Conference on Machine Learning and Applications (ICMLA)*, pp. 94–99, IEEE, 2016.
- [56] A. Kuefler, J. Morton, T. Wheeler, and M. Kochenderfer, "Imitating driver behavior with generative adversarial networks," in *2017 IEEE Intelligent Vehicles Symposium (IV)*, pp. 204–211, IEEE, 2017.
- [57] Y. Li, J. Song, and S. Ermon, "Infogail: Interpretable imitation learning from visual demonstrations," *Advances in Neural Information Processing Systems*, vol. 30, 2017.
- [58] I. Sutskever, O. Vinyals, and Q. V. Le, "Sequence to sequence learning with neural networks," *Advances in neural information processing systems*, vol. 27, 2014.
- [59] C. Zhang, Z. Ni, and C. Berger, "Spatial-temporal-spectral lstm: A transferable model for pedestrian trajectory prediction," *IEEE Transactions on Intelligent Vehicles*, 2023.

- [60] S. Li, Y. Zhou, J. Yi, and J. Gall, "Spatial-temporal consistency network for low-latency trajectory forecasting," in *Proceedings of the IEEE/CVF International Conference on Computer Vision*, pp. 1940–1949, 2021.
- [61] Y. Chai, B. Sapp, M. Bansal, and D. Anguelov, "Multipath: Multiple probabilistic anchor trajectory hypotheses for behavior prediction," *arXiv preprint arXiv:1910.05449*, 2019.
- [62] I. Bae, J.-H. Park, and H.-G. Jeon, "Learning pedestrian group representations for multi-modal trajectory prediction," in *Computer Vision—ECCV 2022: 17th European Conference, Tel Aviv, Israel, October 23–27, 2022, Proceedings, Part XXII*, pp. 270–289, Springer, 2022.
- [63] K. Messaoud, I. Yahiaoui, A. Verroust-Blondet, and F. Nashashibi, "Attention based vehicle trajectory prediction," *IEEE Transactions on Intelligent Vehicles*, vol. 6, no. 1, pp. 175–185, 2020.
- [64] K. Zhang, L. Zhao, C. Dong, L. Wu, and L. Zheng, "Ai-tp: Attention-based interaction-aware trajectory prediction for autonomous driving," *IEEE Transactions on Intelligent Vehicles*, vol. 8, no. 1, pp. 73–83, 2022.
- [65] Z. Li, Y. Wang, and Z. Zuo, "Interaction-aware prediction for cut-in trajectories with limited observable neighboring vehicles," *IEEE Transactions on Intelligent Vehicles*, 2023.
- [66] C. Xu, M. Li, Z. Ni, Y. Zhang, and S. Chen, "Groupnet: Multiscale hypergraph neural networks for trajectory prediction with relational reasoning," in *Proceedings of the IEEE/CVF Conference on Computer Vision and Pattern Recognition*, pp. 6498–6507, 2022.
- [67] L. Shi, L. Wang, C. Long, S. Zhou, M. Zhou, Z. Niu, and G. Hua, "Sgcn: Sparse graph convolution network for pedestrian trajectory prediction," in *Proceedings of the IEEE/CVF Conference on Computer Vision and Pattern Recognition*, pp. 8994–9003, 2021.
- [68] H. Song, D. Luan, W. Ding, M. Y. Wang, and Q. Chen, "Learning to predict vehicle trajectories with model-based planning," in *Conference on Robot Learning*, pp. 1035–1045, PMLR, 2022.
- [69] Y. Chen, B. Ivanovic, and M. Pavone, "Scept: Scene-consistent, policy-based trajectory predictions for planning," in *Proceedings of the IEEE/CVF Conference on Computer Vision and Pattern Recognition*, pp. 17103–17112, 2022.
- [70] T. Phan-Minh, E. C. Grigore, F. A. Boulton, O. Beijbom, and E. M. Wolff, "Covernet: Multimodal behavior prediction using trajectory sets," in *Proceedings of the IEEE/CVF Conference on Computer Vision and Pattern Recognition*, pp. 14074–14083, 2020.
- [71] L. F. Chiara, P. Coscia, S. Das, S. Calderara, R. Cucchiara, and L. Ballan, "Goal-driven self-attentive recurrent networks for trajectory prediction," in *Proceedings of the IEEE/CVF Conference on Computer Vision and Pattern Recognition*, pp. 2518–2527, 2022.
- [72] J. Wang, T. Ye, Z. Gu, and J. Chen, "Ltp: Lane-based trajectory prediction for autonomous driving," in *Proceedings of the IEEE/CVF Conference on Computer Vision and Pattern Recognition*, pp. 17134–17142, 2022.
- [73] J. Gu, C. Sun, and H. Zhao, "Densetnt: End-to-end trajectory prediction from dense goal sets," in *Proceedings of the IEEE/CVF International Conference on Computer Vision*, pp. 15303–15312, 2021.
- [74] W. Mao, C. Xu, Q. Zhu, S. Chen, and Y. Wang, "Leapfrog diffusion model for stochastic trajectory prediction," in *Proceedings of the IEEE/CVF Conference on Computer Vision and Pattern Recognition*, pp. 5517–5526, 2023.
- [75] X. L. Li, J. Thickstun, I. Gulrajani, P. Liang, and T. B. Hashimoto, "Diffusion-lm improves controllable text generation," *arXiv preprint arXiv:2205.14217*, 2022.
- [76] Y. Tashiro, J. Song, Y. Song, and S. Ermon, "Csdi: Conditional score-based diffusion models for probabilistic time series imputation," *Advances in Neural Information Processing Systems*, vol. 34, pp. 24804–24816, 2021.
- [77] J. Sohl-Dickstein, E. Weiss, N. Maheswaranathan, and S. Ganguli, "Deep unsupervised learning using nonequilibrium thermodynamics," in *International Conference on Machine Learning*, pp. 2256–2265, PMLR, 2015.
- [78] L. Yang, Z. Zhang, Y. Song, S. Hong, R. Xu, Y. Zhao, Y. Shao, W. Zhang, B. Cui, and M.-H. Yang, "Diffusion models: A comprehensive survey of methods and applications," *arXiv preprint arXiv:2209.00796*, 2022.
- [79] D. J. Rezende, S. Mohamed, and D. Wierstra, "Stochastic backpropagation and approximate inference in deep generative models," in *International conference on machine learning*, pp. 1278–1286, PMLR, 2014.
- [80] I. Goodfellow, J. Pouget-Abadie, M. Mirza, B. Xu, D. Warde-Farley, S. Ozair, A. Courville, and Y. Bengio, "Generative adversarial networks," *Communications of the ACM*, vol. 63, no. 11, pp. 139–144, 2020.
- [81] H. Cao, C. Tan, Z. Gao, G. Chen, P.-A. Heng, and S. Z. Li, "A survey on generative diffusion model," *arXiv preprint arXiv:2209.02646*, 2022.
- [82] C. Luo, "Understanding diffusion models: A unified perspective," *arXiv preprint arXiv:2208.11970*, 2022.
- [83] I. Bae, J.-H. Park, and H.-G. Jeon, "Non-probability sampling network for stochastic human trajectory prediction," in *Proceedings of the IEEE/CVF Conference on Computer Vision and Pattern Recognition*, pp. 6477–6487, 2022.